On the Accuracy of Force Fields for Predicting the Physical Properties of Dimethylnitramine

Lianqing Zheng and Donald L. Thompson*

Department of Chemistry, University of Missouri, Columbia, Missouri 65211

Received: March 23, 2006; In Final Form: June 1, 2006

The accuracy of three force fields for predicting the physical properties of dimethylnitramine (DMNA) has been investigated by using molecular dynamics simulations. The Sorescu, Rice, and Thompson (SRT) (*J. Phys. Chem. B* **1997**, *101*, 798) rigid-molecule, flexible generalized AMBER (*J. Comput. Chem.* **2004**, *25*, 1157), and Smith et al. flexible force fields (*J. Phys. Chem. B* **1999**, *103*, 705) were tested. The density, lattice parameters, isotherm, and melting point of DMNA are calculated using classical molecular dynamics. Except for the melting point, the predictions of the three force fields are in reasonable agreement with experimental values. The calculated thermodynamic melting points (T_{mp}) for the SRT, AMBER, and Smith et al. force fields are 380, 360, and 260 K, respectively. The experimental value is 331 K. Modifications of the torsional barriers in the AMBER force field resulted in $T_{mp} = 346$ K, in good agreement with the experimental value of 331 K. The calculated lattice parameters and bulk modulus are also improved with the modifications of the AMBER potential. The results indicate that, although not sufficiently accurate without modifications, the general force fields such as AMBER provide the basis for developing force fields that correctly predict the physical properties of nitramines.

I. Introduction

Accurate force fields are needed for molecular dynamics (MD) simulations. Force fields are usually formulated by using a combination of experimental and theoretical data for the crystal structure, lattice energy, vibrational frequencies, molecular geometry, and other equilibrium properties, and they are usually validated by comparisons with measured equilibrium properties. We are interested in using force fields in simulations of physical processes for energetic materials composed of H, C, N, and O over wide ranges of temperature and pressure and for nonequilibrium conditions. A reasonable way to develop these force fields is to begin with existing force fields, which have undergone some validation. If we can determine the critical features of force fields that determine the properties of interest, then relatively straightforward procedures for modifying the existing force fields can be formulated. We begin with the simplest of compounds of interest to us, dimethylnitramine, $(CH_3)_2NNO_2$. We report the results of a study in which MD simulations have been used to determine the critical features of force fields that determine the accuracy of predictions of the density, lattice parameters, isotherm, and melting point.

Dimethylnitramine is often used as a prototype of more important energetic materials such as RDX (hexahydro-1,3,5-trinitro-1,3,5-*s*-triazine) and HMX (octahydro-1,3,5,7-tetranitro-1,3,5,7-tetraazacyclooctane). Dimethylnitramine (DMNA) belongs to the $P2_1/m$ ($Z = 2$) space group with a planar molecular skeleton of C_{2v} symmetry under ambient conditions.[1,2] It melts at 331 K at 1 atm.[1] Rey-Lafon and co-workers[3−6] performed a series of infrared and Raman spectroscopy experiments to determine the vibrational frequencies of DMNA. The structure of gas-phase DMNA has been determined to be planar on the basis of electron diffraction experiments,[7] although a nonplanar structure could not be totally rejected.[7,8] Quantum-chemistry calculations predict the ground state of the molecule to be nonplanar and of C_s symmetry, with the predictions of the $N-NC_2$ wag varying from ∼30 to ∼40° depending on the level of theory.[8,9] This discrepancy between experiment and calculations is explained by the small inversion barrier (∼4.0 kJ/mol)[8,9] of the C−N−C group of DMNA.[9] Illustrations of the crystal-phase DMNA molecular configuration and three side views of the crystal ($4 \times 4 \times 5$ unit cells) under ambient conditions are shown in Figure 1. The coordinates of the atoms used to make these illustrations were taken from ref 1. The labels on the atoms in Figure 1a will be used in the discussions that follow.

Several reviews of MD simulations of energetic materials have been reported recently[10−12] that illustrate the need to develop accurate force fields for modeling the properties and processes of energetic materials. Although the interest in energetic materials is primarily on their chemical reactivity, it is critical that theoretical models accurately describe the physical properties and processes, which are important underlying factors in the chemical behavior. There is good evidence from many experimental studies that the chemistry is strongly influenced and even preceded by physical changes in the materials. An acceptable force field must correctly describe not only the fundamental properties such as density, structures, and phonon spectra but also solid−solid, solid−liquid, solid−vapor, and liquid−vapor transitions. Crystalline phase transitions are probably the largest challenge, with melting being the next most difficult physical process to correctly model. We have had some limited success simulating melting using a rigid force field,[13] but clearly, molecular flexibility affects the behavior of most materials. For example, a rigid-molecule force field fails to realistically model the melting of cyclic nitramines.[14] Our goal in the present study was to investigate the accuracy of various force fields in melting simulations of the simple prototypical

* Corresponding author. E-mail: thompsondon@missouri.edu.

10.1021/jp061810l CCC: $33.50
Published on Web 07/21/2006

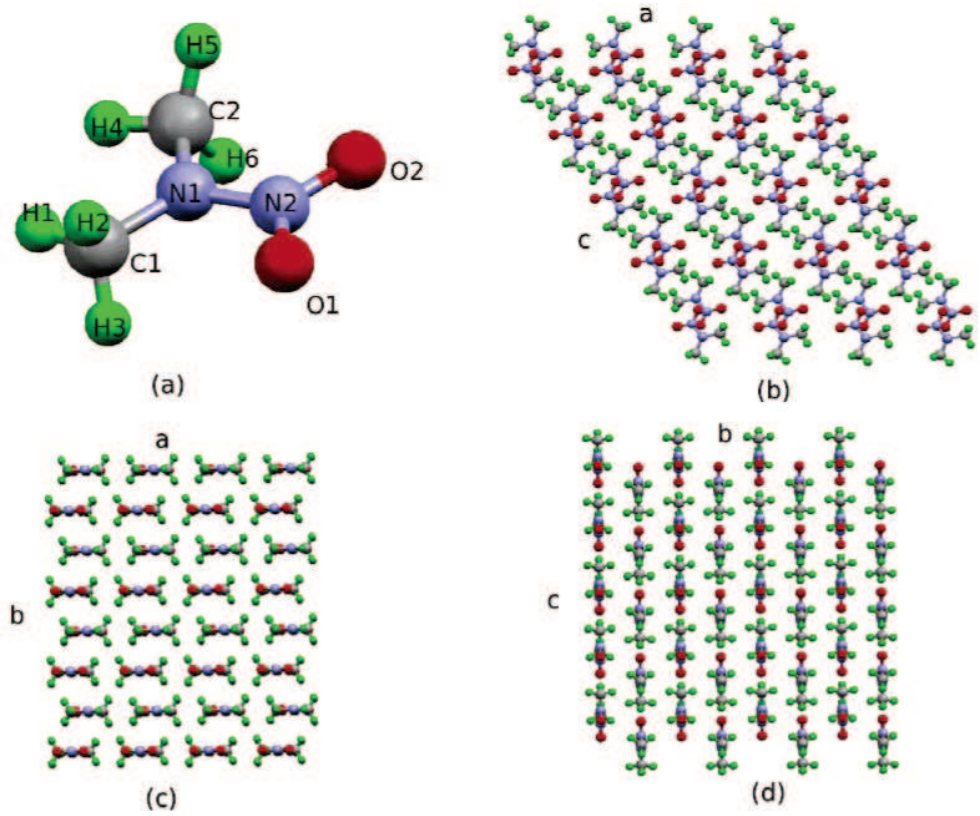

Figure 1. Configurations of the DMNA molecule (a) and crystal (b−d) under ambient conditions. The atomic coordinates are taken from ref 1. Shown in parts b−d are three side views of a 4 × 4 × 5 DMNA supercell. The C, N, O, and H atoms are shown in gray, blue, red, and green colors, respectively.

nitramine DMNA. The more general goal is to determine how existing force fields can be modified to predict melting points.

The first MD simulations of DMNA were done in the 1980's by Sumpter and Thompson[15,16] to study the gas-phase dissociation of DMNA. More recently, MD studies have focused on the physical properties of DMNA. Kohno, Ueda, and Imamura[17] constructed force fields for DMNA and cyclic nitramines using CHARMM22[18] and ab initio calculations at the MP2/4-31G level, which have been used in MD simulations by Ye et al.[19] Smith, Bharadwaj, Bedrov, and Ayyagari[9] (hereafter, SBBA) developed a force field and used it in gas- and liquid-phase simulations of DMNA. The SBBA force field has been extended to describe HMX[20] and used to compute the thermal conductivity,[21] shear viscosity coefficient,[22] lattice parameters, coefficients of thermal expansion,[23] and elastic properties.[24] Sorescu, Rice, and Thompson[25] (hereafter, SRT) have developed a rigid-molecule potential for nitramine crystals,[26] which accurately predicts crystal densities, lattice parameters, thermal expansion coefficients, and isotherms with moderate increases in pressure and temperature.[27] They have added intramolecular terms to the rigid-molecule model to obtain a fully flexible force field for nitromethane[28] that predicts the harmonic vibrational frequencies, lattice parameters, thermal expansion, isotherm, and melting point[13] in excellent agreement with experimental results.

In the present study, we examine three force fields for use in MD simulations of the physical properties of DMNA: the SRT rigid-molecule,[25] generalized AMBER,[29] and SBBA force fields.[9] We began by testing these force fields to determine their accuracy in predictions of the fundamental physical properties of the condensed phases including melting. The SRT force field is a rigid-molecule model that is simple in form and accurately predicts many of the physical properties of a wide range of energetic crystals at moderate temperatures and pressures. We take the AMBER force field to be representative of general force fields. It is fully flexible, and the parameters are easily obtained from its database. We modified the AMBER force field to obtain more accurate simulation results. We take the SBBA force field to be typical of custom-designed, quantum-chemistry-based force fields. We have not included the Kohno et al.[17] force field in the study because the values of some of the parameters are not available in the literature.

TABLE 1: Partial Charges (units, *e*) for the SRT, AMBER, and SBBA Potentials

atom[a]	SRT[b]	AMBER[c]	SBBA[d]
C1	−0.057 624	−0.076 694	−0.618 06
C2	−0.239 333	−0.309 918	−0.618 06
N1	−0.097 975	−0.014 662	−0.085 46
N2	0.777 009	0.672 382	0.840 66
O1	−0.494 879	−0.462 924	−0.469 70
O2	−0.488 435	−0.454 766	−0.469 70
H1	0.089 756	0.089 628	0.236 72
H2	0.069 364	0.070 636	0.236 72
H3	0.069 364	0.070 636	0.236 72
H4	0.140 223	0.151 876	0.236 72
H5	0.116 265	0.131 903	0.236 72
H6	0.116 265	0.131 903	0.236 72

[a] The atom labels are defined in Figure 1a. [b] Calculated by using the CHELPG method in Gaussian 03 at the MP2/6-31G** level.[25] [c] Calculated by using the RESP method at the MP2/6-31** level.[29] [d] Taken from Smith et al.[9]

II. Computational Methods

A. Potentials. The SRT potential[25] contains only intermolecular terms:

$$U^{\mathrm{SRT}} = \sum_{i=1}^{N}\sum_{j=i+1}^{N}\left(k_c\frac{q_iq_j}{r_{ij}} + A_{ij}e^{-B_{ij}r_{ij}} - \frac{C_{ij}}{r_{ij}^{6}}\right) \quad (1)$$

where k_c is the Coulomb constant, N is the number of atoms, r_{ij} is the distance between atoms i and j, and A_{ij}, B_{ij}, and C_{ij} are parameters. The partial charges (q_i) (see column 2 of Table 1) were obtained by using the procedure described in ref 25; that is, they were calculated using the CHELPG method in Gaussian 03[30] at the MP2/6-31G** level. The molecular structure of DMNA was taken from experiment.[1] The SRT force field has been validated for many physical properties of a number of systems.[26]

The AMBER potential[29] has the form

$$U^{\mathrm{Amber}} = \sum_{i=1}^{N}\sum_{j=i+1}^{N}\left(k_c\frac{q_iq_j}{r_{ij}} + \frac{A_{ij}}{r_{ij}^{12}} - \frac{B_{ij}}{r_{ij}^{6}}\right) + \sum_{\mathrm{bonds}}\frac{K^S}{2}(r-r^0)^2 + \sum_{\mathrm{angles}}\frac{K^B}{2}(\theta-\theta^0)^2 + \sum_{\mathrm{dihedrals}}K^T[1+\cos(n\phi-\phi^0)] \quad (2)$$

where r, θ, and ϕ are the bond lengths, bond angles, and dihedral angles, respectively. The partial charges (q_i) were obtained using the RESP (restrained electrostatic potential fit) method at the MP2/6-31** level for the experimentally determined molecular structure.[1] The HCNN and CNNO torsional barriers in DMNA computed by using the AMBER database differ significantly from those predicted by quantum-chemistry calculations;[8,9] thus, modifications in the potential, which are discussed in the following section, were made to give better agreement for torsional barriers. Simulations were performed using both the unmodified and modified AMBER potentials.

The functional form of the SBBA potential[9] is the same as the AMBER potential except for an additional term that describes the out-of-plane (δ) motion of the nitro group:

$$U^{\mathrm{SBBA}} = \sum_{i=1}^{N}\sum_{j=i+1}^{N}\left(k_c\frac{q_iq_j}{r_{ij}} + A_{ij}e^{-B_{ij}r_{ij}} - \frac{C_{ij}}{r_{ij}^{6}}\right) + \sum_{\mathrm{bonds}}\frac{K^S}{2}(r-r^0)^2 + \sum_{\mathrm{angles}}\frac{K^B}{2}(\theta-\theta^0)^2 + \sum_{\mathrm{dihedrals}}K^T[1+\cos(n\phi-\phi^0)] + \sum_{\text{out-of-plane bends}}\frac{K^O}{2}\delta^2 \quad (3)$$

This is a quantum-chemistry-based fully flexible force field. We have used it without modifications. A complete description of the force field is given in ref 9.

The partial charges for the SRT, AMBER, and SBBA force fields are given in columns 2, 3, and 4, respectively, of Table 1. The values of the parameters for the van der Waals interactions in the SBBA, SRT, and AMBER potentials were taken from refs 9, 25, and 31, respectively. The values of the parameters for the intramolecular terms in the AMBER and SBBA force fields are given in Table 2.

B. Molecular Dynamics Simulations. We performed MD simulations for Nosé−Hoover constant-temperature and constant-pressure (NPT) ensembles[32−34] with 3-D boundary conditions using DL_POLY 2.14[35] and GROMACS 3.2.[36−38] The relaxation times for the thermostat and barostat were both 1.0 ps. The initial configuration of DMNA (see Figure 1) is from the crystallographic data.[1] The simulation supercell was 4 × 4 × 5 unit cells (160 molecules, 1920 atoms). The integration time step was 1.0 fs. The cutoff distance for the van der Waals interactions was 10.0 Å. The electrostatic interactions were calculated using the smooth particle mesh Ewald algorithm.[39] The velocities of the atoms were assigned to give a particular temperature.[40,41] The system was then equilibrated with temperature scaling for 100 ps at 1 atm, and the properties were computed by using averages for the remaining duration of the simulation, which ranged from 400 ps to 1.4 ns.

TABLE 2: Intramolecular Parameters for the AMBER and SBBA Potentials

Bond Stretches

	AMBER		SBBA[a]	
bond type	K_{ij}^S (kJ/mol/Å^2)	r_{ij}^0 (Å)	K_{ij}^S (kJ/mol/Å^2)	r_{ij}^0 (Å)
O−N	6369.72	1.219	8326.58	1.23
N−N	3301.18	1.445	4149.27	1.36
N−C	2682.78	1.470	2812.07	1.44
C−H	2810.81	1.093	2684.45	1.09

Angle Bends

	AMBER		SBBA	
bend type	K_{ijk}^B (kJ/mol/rad^2)	θ_{ijk}^0 (deg)	K_{ijk}^B (kJ/mol/rad^2)	θ_{ijk}^0 (deg)
O−N−O	623.3152	127.55	523.0	120.92
O−N−N	602.4960	115.56	523.0	107.45
N−N−C	552.2880	111.27	543.92	95.82
C−N−C	535.5520	110.90	292.88	105.60
N−C−H	410.0320	109.92	361.50	107.01
H−C−H	328.0256	109.55	322.17	108.51

Torsions[b]

	AMBER		SBBA	
torsion type	K_{ijkl}^T (kJ/mol)	n	K_{ijkl}^T (kJ/mol)	n
O−N−N−C	16.736	2	17.6774	2
O−N−N−C			1.6527	4
O−N−N−C			0.008368	8
H−C−N−C	1.2552	3 ($\phi^0 = 0°$)	−0.3347	3
H−C−N−N	1.2552	3 ($\phi^0 = 0°$)		

Out-of-Plane Bend

	AMBER	SBBA
out-of-plane bend type	K_{ijkl}^O (kJ/mol/rad^2)	K_{ijkl}^O (kJ/mol/rad^2)
O−N−O−*N		373.8156

[a] Taken from Smith et al.[9] [b] $\phi^0 = 180°$ if not otherwise stated.

The melting point is taken to be the temperature at which the volume of the simulation cell and the diffusion coefficient increase sharply. To preclude superheating and thus obtain the thermodynamic melting point (T_{mp}), voids were introduced into the simulation supercell by removing randomly selected molecules.[13,40,41] The thermodynamic melting point is taken to be the temperature of the plateau region of the calculated melting point versus the number of voids,[42,43] that is, the region where the melting point is independent of the number of voids. To compute the isothermal $P-V$ curve, we applied "instantaneous" pressure[44] on the configuration obtained experimentally[1] at 1 atm; that is, the equilibration simulations were carried out for different pressures. The experimental bulk modulus (B) of DMNA was calculated by fitting the $P-V$ curve to the Murnaghan equation:[4]

$$P = \frac{B}{B'}\left[\left(\frac{V_0}{V}\right)^{B'} - 1\right] \quad (4)$$

TABLE 3: Calculated Lattice Parameters and Density of Crystalline DMNA and Density of Liquid DMNA Compared to Other MD Results and Experimental Data

	SRT[a]	AMBER[a]	SBBA[a]	other MD[b]	expt[c]
a (Å)	6.59	6.61	6.46	6.61	6.587
b (Å)	6.47	6.46	6.57	6.26	6.500
c (Å)	6.11	6.22	5.93	6.23	6.131
α (deg)	90.03	90.23	88.76	90.0	90.0
β (deg)	122.74	123.39	119.98	123.84	123.13
γ (deg)	90.06	90.08	88.19	90.0	90.0
density (solid) (g/cm^3)	1.363	1.348	1.375	1.395	1.36
density (liquid) (g/cm^3)	1.05[d]	1.11[d]	1.16[e]	1.07[f]	1.10[g]

[a] $T = 300$ K and $P = 1$ atm if not otherwise mentioned. [b] Ye et al.[19] except for the density of the liquid. [c] Filho et al.[1] under ambient conditions except for the density of liquid. [d] $T = 400$ K and $P = 1$ atm, from a supercell with 16 voids. [e] $T = 400$ K and $P = 1$ atm, from a perfect supercell. [f] From Smith et al.,[9] $T = 400$ K, and the supercell contained 108 DMNA molecules. [g] Lide,[45] $T = 350$ K.

where P is the pressure, B' is the pressure derivative of B, V is the volume, and V_0 is the volume at zero pressure. We used the same approach to calculate B from the simulation results.

III. Results and Discussion

The values of the lattice parameters and the densities of crystalline and liquid DMNA calculated using the SRT, unmodified AMBER, and SBBA force fields are given in Table 3 (columns 2, 3, and 4, respectively). The MD results of Ye et al.[19] for the solid and the value of the liquid density computed by Smith et al.[9] are given in column 5 of Table 3; the experimental results[1] are given in column 6. All of the computed results for the solid are in good agreement with experiment, with absolute deviations varying from 0.1 to 3.3%. The SRT potential predicts a value of the density of crystalline DMNA that is about 0.2% higher than the experimental value, while the AMBER and SBBA force fields give values that are, respectively, about 0.9% lower and 1.1% higher. The SRT potential gives the best results with the largest error of only 0.5% (for the length of cell edge b), compared to 1.5 and 3.3% for, respectively, the AMBER and SBBA potentials (in both cases for the length of cell edge c). Using the Kohno et al.[17] force field, Ye et al.[19] calculated the lattice parameters and density (see column 5 of Table 3). The deviations from experiment of the lengths of the unit cell edges a, b, and c are 0.3, −3.7, and 1.6%, respectively, and that for the density is 2.6%. The experimental value[45] of the density at 350 K is smaller than the values computed at 400 K using the AMBER and SBBA force fields. A previous MD simulation of liquid DMNA[9] using the SBBA force field gave a density that is about 8% lower than the value we calculated. A smaller simulation cell (108 molecules compared to 160 in the present study) was used in that study;[9] thus, we have investigated the influence of the simulation cell size to see if that might account for the difference. For a direct comparison, we performed a simulation at 400 K using a supercell with the same number of molecules (108), 3 × 3 × 6 unit cells with dimensions of 19.74 × 19.5 × 36.78 Å^3. A cutoff distance of 8 Å was used so that the simulation cell edges were at least twice the cutoff distance. The calculated density is 1.17 g/cm^3, which is almost identical to the value we calculated (1.16 g/cm^3) using the larger supercell. The discrepancy does not appear to be due to different simulation cell sizes or to other simulation parameters. We have been unable to determine the cause of the discrepancy between our results and those of the previous study.

Figure 2 shows the variations in the unit cell volume and the lengths of the unit cell edges with applied hydrostatic pressure

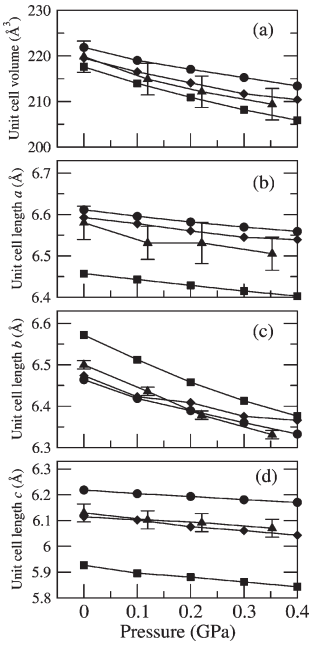

Figure 2. Dependences of the unit cell volume (a) and unit cell edge lengths (b−d) of crystalline DMNA as functions of applied hydrostatic pressures: simulation results using the SRT (diamonds), AMBER (circles), and SBBA (squares) potentials and experiment (triangles).[4] The MD simulations are for 300 K, and the experimental data are for 293 K.

up to 0.4 GPa at 300 K. The deviation of the unit cell volume calculated with the SRT potential from the experimental values increases from 0.2 to 0.8% with increasing pressure. The unit cell volumes predicted by the AMBER potential are systematically larger than the experimental values as the pressure increases, and the deviations increase from 0.9% at 1 atm to ∼2.4% at 3.5 GPa, while the results for the SBBA potential are systematically smaller than experiment—the deviations remain almost constant at ∼1.0%. Considering the error bars for the experimental data, all of the simulation results are in good agreement. The lengths of unit cell edge a calculated using the SRT potential deviate less than 0.6% from the experimental values, and those from the AMBER and SBBA potentials deviate by about 1.0 and 1.5%, respectively. The SBBA potential gives results for cell edge b that are consistently ∼1.0% larger than the experimental ones, while the deviations of the AMBER potential results vary from −0.6 to +0.3%. The length of cell edge b predicted by the SRT potential is about 0.5% lower than the experimental value at 1 atm, and the deviation is 0.6% higher at ∼0.35 GPa. The deviations from experiment of the lengths of unit cell edge c calculated using the AMBER and SBBA force fields are, respectively, about 1.5 and −3.6%, while those predicted by the SRT potential vary from −0.3 to 0.3% with increasing pressure.

The values of the bulk modulus and pressure derivative for crystalline DMNA obtained by fitting the $P-V$ curves to the Murnaghan equation, eq 4, are given in Table 4, along with the experimental data[4] and the Ye et al.[19] results for $T = 298$ K. The bulk modulus predicted by the SRT potential is closest (5.7% lower) to the experimental value, while the AMBER potential gives a value that is 16.6% higher and the SBBA potential gives a value that is 15.8% smaller. Ye et al.[19] computed a value of 11.3 GPa for the bulk modulus using the Kohn et al. potential,[17] which is substantially larger (73.8%) than the experimental value of 6.5 ± 0.3 GPa.[4]

TABLE 4: Bulk Modulus and Pressure Derivative of Crystalline DMNA

force field	B (GPa)	B'
SRT	6.13	18.3
AMBER	7.58	15.4
SBBA	5.47	9.6
Kohno et al.[a]	11.3	7.2
experiment[b]	6.5 ± 0.3	8 ± 2

[a] Calculated by Ye et al.[19] using $B = 1/V(d^2U/dV^2)$ at 298 K. [b] Rey-Lafon et al.[4]

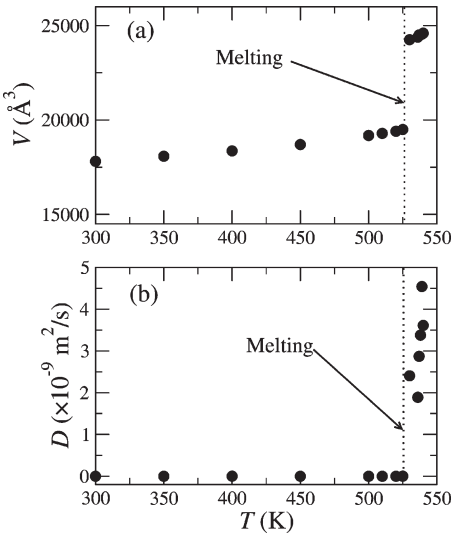

Figure 3. (a) Simulation supercell volume (V) and (b) diffusion coefficient (D) as functions of temperature for perfect crystals. The calculations were done by using the AMBER potential.

The measured melting point of DMNA at 1 atm is 331 K.[1] The computed values of the melting point of the perfect DMNA crystal (i.e., the maximum superheating temperature (T_s)) are 531, 525, and 366 K for the SRT, AMBER, and SBBA potentials, respectively. The melting point is taken to be the temperature at which the simulation cell volume (V) and diffusion coefficient (D) undergo abrupt changes. The results obtained using the AMBER potential are shown in Figure 3. The thermodynamic melting point is approached by introducing voids in the crystal, which decreases the nucleation energy barrier. The melting point decreases with increasing number of voids, levels off, and then drops abruptly when enough voids are introduced to render the crystal structure unstable. We calculated properties for each simulation to ascertain that the simulated solid remained crystalline until it melted. The system did not pass through an amorphous state prior to melting for the various numbers of voids that we studied. Figure 4 shows the calculated values of the melting point versus the number of voids for the SRT, AMBER, and SBBA potentials. The plateau regions occur for 13−16 voids for the SRT and SBBA potentials (see, respectively, parts a and c of Figure 4) and for 16−19 voids for the AMBER potential (see Figure 4b). Due to the small statistical errors in the simulation results, the plateau is only approximately level; thus, we averaged the values in the plateau regions to obtain the values of the thermodynamic melting point. The values of the melting point computed using the SRT and AMBER potentials are, respectively, 380 and 361 K (respectively, ∼15 and ∼9% higher than the experimental value). The value obtained by using the SBBA potential is 260 K, substantially lower than the experimental value. The extent of superheating (T_s/T_{mp}) is 1.40, 1.45, and 1.41 for the SRT, AMBER, and SBBA potentials, respectively. All of these values

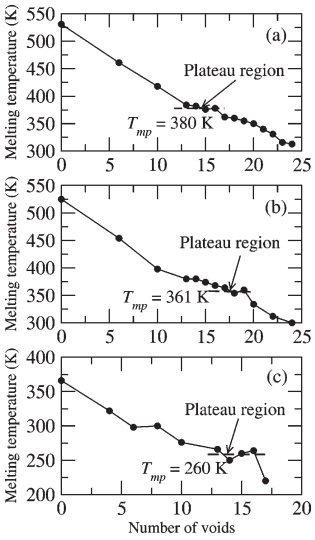

Figure 4. Computed melting point as a function of the number of voids for the (a) SRT, (b) AMBER, and (c) SBBA potentials. The thermodynamic melting point is taken to be the temperature of the plateau region, which is shown by the horizontal line in each frame.

are considerably larger than those found in atomic solids[46] and relatively rigid molecules such as nitromethane,[13] most of which are in a range of ∼0.15−0.25. This indicates that the limit of superheating in DMNA is greater than that for these simpler solids, which may be due to a higher solid−liquid interfacial energy.

Although the AMBER and SBBA potentials are similar in many respects (e.g., compare the parameters in Table 2), they predict values of the thermodynamic melting point that differ by ∼100 K (360 and 260 K, respectively). The main difference in the two potentials is the HCNN and CNNO torsional barriers. Following the rule of the AMBER force field,[29] we determined the torsional barrier of a dihedral angle to be $2K^T$ multiplied by the number paths (K^T is defined in eq 2). For example, K^T = 16.736 kJ/mol and the number of paths is 4 for the CNNO dihedral; therefore, the barrier is 133.888 kJ/mol. The values of the HCNN barrier in the SBBA and AMBER potentials are ∼2.0 and ∼15.0 kJ/mol, respectively; quantum-chemistry calculations predict the methyl group torsional barrier to be ∼6.8 kJ/mol.[9] Experimentally, the CNNO torsional barrier height has been determined to be 37.7 kJ/mol or larger.[47] Recent quantum-chemistry calculations predict barrier heights of 40.6 kJ/mol at the MP2/6-31G* level[8] and 44.3 kJ/mol at the MP2/6-311G-(2df,2p)//MP2/6-311G** level.[9] The CNNO torsional barrier heights for the AMBER and SBBA force fields are, respectively, 133.9 and 141.4 kJ/mol.

Our interest is in determining whether (and how) the general AMBER force field can be used as a starting point for developing force fields for nitramine energetic materials; thus, we made modifications in it to obtain more accurate barriers for the torsional motions (see below). We did not attempt modifications of the SBBA force field; rather, we focused on the more general AMBER potential. Adjustments of the torsional barrier heights in the AMBER force field led to significant improvement in the agreement with experiment, while the behavior of the melting point as a function of the number of voids was not noticeably changed; compare the results in Figures 4b and 5. We changed the HCNN and CNNO torsional barriers in the AMBER potential to 6.8 and 46.0 kJ/mol, respectively. The melting point of the perfect crystal drops from 525 to 488 K as a result of this change. The calculated melting point as a

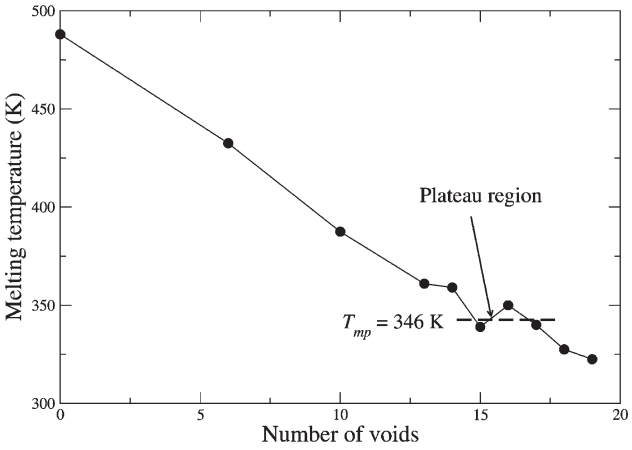

Figure 5. Computed melting point as a function of the number of voids from the modified AMBER potential.

function of the number of voids is shown in Figure 5. The plateau region occurs for 15 to 17 voids to give 346 K for the thermodynamic melting point, which is in much better agreement with the experimental value of 331 K. Further study is needed to draw a general conclusion; however, the present study indicates that accurate simulations of the melting of polyatomic materials require that the molecular flexibility be realistically described.

Finally, we note that the plateau region (the range of the number of void defects for which the melting temperature is essentially constant) is not as well defined as in the cases of the Lennard-Jones system[48] and relatively rigid, small molecules such as nitromethane.[13] This is probably due to the difficulty of minimizing the statistical error in simulations of the flexible DMNA molecule.

The modified AMBER potential predicts 1.345 g/cm^3 for the crystal density at 300 K and 1 atm, about the same as the value computed with the unmodified AMBER potential, thus also somewhat smaller than the measured value (1.36 g/cm^3). The calculated unit cell edge lengths are 6.57, 6.54, and 6.19 Å for deviations from experiment of −0.3, 0.6, and 1.0% for edges *a*, *b*, and *c*, respectively, which are better results than those obtained with the original potential (see column 3 of Table 3). The modified AMBER potential also gives a better value of the bulk modulus, 7.23 GPa, compared to that predicted by the unmodified AMBER potential, 7.58 GPa, and the measured value is 6.5 GPa.[4]

IV. Summary and Conclusions

We have investigated the accuracy of existing force fields, and suggested modifications, for predicting the physical properties, including melting, of dimethylnitramine. Specifically, we performed MD simulations using the rigid-molecule model developed by Sorescu, Rice, and Thompson,[25] the generalized AMBER force field,[29] and a quantum-chemistry-based force field developed by Smith and co-workers.[9] The lattice parameters, densities, isotherms, and melting points were calculated; all three force fields give results in reasonable accord with experiment, particularly the density and lattice parameters, which are within 3.3% of the experimental values. However, there are large disagreements in the predicted values of the thermodynamic melting point: 380, 361, and 260 K, from the SRT, AMBER, and SBBA potentials, respectively, compared to the experimental value of 331 K. The fault appears to lie in the descriptions of the torsional barriers. The HCNN and CNNO torsional barrier heights in the AMBER and SBBA potentials differ significantly with the experimental and quantum-chemistry values. Our interest is to arrive at a general method for formulating accurate force fields for the entire class of nitramines; thus, we chose to modify the AMBER potential torsional barriers to make them comparable to the experimental and quantum-chemistry ones. The modified AMBER force field predicts 346 K for the thermodynamic melting point compared to the experimental value of 331 K. Also, better agreement with experiment for the lattice parameters and bulk modulus was obtained with the modified AMBER potential. While more studies are needed for a general conclusion, these results suggest that it is crucial that the torsional motions of flexible molecules be accurately described for accurate predictions of melting points, although many other physical properties appear to not be strongly affected by inaccurate intramolecular interactions (the rigid-molecule SRT force field accurately predicts them!).

Acknowledgment. This work was supported by a MURI grant managed by the Army Research Office. We thank Drs. Saman Alavi, Yin Guo, Betsy M. Rice, and Thomas D. Sewell for helpful discussions.

References and Notes

(1) Filhol, A.; Bravic, G.; Rey-Lafon, M.; Thomas, M. *Acta Crystallogr.* **1980**, *B36*, 575.
(2) Krebs, B.; Mandt, J.; Cobbledick, R. E.; Small, R. W. H. *Acta Crystallogr.* **1979**, *B35*, 402.
(3) Rey-Lafon, M. *J. Chem. Phys.* **1979**, *71*, 5324.
(4) Rey-Lafon, M.; Filhol, A.; Jobic, H. *J. Phys. Chem. Solids* **1983**, *44*, 81.
(5) Trinquecoste, C.; Rey-Lafon, M.; Forel, M.-T. *Spectrochim. Acta* **1974**, *30A*, 813.
(6) Trinquecoste, C.; Rey-Lafon, M.; Forel, M.-T. *Can. J. Spectrosc.* **1974**, *19*, 75.
(7) Stolevik, R.; Rademacher, P. *Acta Chem. Scand.* **1969**, *23*, 672.
(8) Khaikin, L. S.; Grikina, O. E.; Perevozchikov, V. I.; Abramenkov, A. V.; Shlyapochnikov, V. A.; Cordell, F. R.; Boggs, J. E. *Russ. Chem. Bull.* **1998**, *47*, 213.
(9) Smith, G. D.; Bharadwaj, R. K.; Bedrov, D.; Ayyagari, C. *J. Phys. Chem. B* **1999**, *103*, 705.
(10) Rice, B. M. In *Modern Methods for Multidimensional Dynamics Computations in Chemistry*; Thompson, D. L., Ed.; World Scientific Publishing Co.: Singapore, 1998; pp 472−528.
(11) Sorescu, D. C.; Rice, B. M.; Thompson, D. L. In *Energetic Materials. Part 1. Decomposition, Crystal and Molecular Properties*; Politzer, P., Murray, J. S., Eds.; Elsevier: Amsterdam, The Netherlands, 2003; pp 125−184.
(12) Holian, B. L.; Germann, T. C.; Strachan, A.; Maillet, J.-B. In *Chemistry at Extreme Conditions*; Manaa, M. R., Ed.; Elsevier: Amsterdam, The Netherlands, 2005; pp 269−296.
(13) Agrawal, P. M.; Rice, B. M.; Thompson, D. L. *J. Chem. Phys.* **2003**, *119*, 9617.
(14) Agrawal, P. M.; Rice, B. M.; Thompson, D. L. Unpublished results.
(15) Sumpter, B. G.; Thompson, D. L. *J. Chem. Phys.* **1987**, *86*, 3301.
(16) Sumpter, B. G.; Thompson, D. L. *J. Chem. Phys.* **1988**, *88*, 6889.
(17) Kohno, Y.; Uede, K.; Imamura, A. *J. Phys. Chem.* **1996**, *100*, 4701.
(18) Brooks, B. R.; Bruccoleri, R. E.; Olafson, B. D.; States, D. J.; Swaminathan, S.; Karplus, M. J. *J. Comput. Chem.* **1983**, *4*, 187.
(19) Ye, S.; Tonokura, K.; Koshi, M. *Kayaku Gakkaishi* **2002**, *63*, 104.
(20) Smith, G. D.; Bharadwaj, R. K. *J. Phys. Chem. B* **1999**, *103*, 3570.
(21) Bedrov, D.; Smith, G. D.; Sewell, T. D. *Chem. Phys. Lett.* **2000**, *324*, 64.
(22) Bedrov, D.; Smith, G. D.; Sewell, T. D. *J. Chem. Phys.* **2000**, *112*, 7203.
(23) Bedrov, D.; Ayyagari, C.; Smith, G. D.; Sewell, T. D.; Menikoff, R.; Zaug, J. M. *J. Comput.-Aided Mater. Des.* **2001**, *8*, 77.
(24) Sewell, T. D.; Menikoff, R.; Bedrov, D.; Smith, G. D. *J. Chem. Phys.* **2003**, *119*, 7417.
(25) Sorescu, D. C.; Rice, B. M.; Thompson, D. L. *J. Phys. Chem. B* **1997**, *101*, 798.
(26) Sorescu, D. C.; Rice, B. M.; Thompson, D. L. *J. Phys. Chem. A* **1998**, *102*, 8386.
(27) Sorescu, D. C.; Rice, B. M.; Thompson, D. L. *J. Phys. Chem. B* **1999**, *103*, 6783.
(28) Sorescu, D. C.; Rice, B. M.; Thompson, D. L. *J. Phys. Chem. B* **2000**, *104*, 8406.

(29) Wang, J.; Wolf, R. M.; Caldwell, J. W.; Kollman, P. A.; Case, D. A. *J. Comput. Chem.* **2004**, *25*, 1157.
(30) Frisch, M. J.; et al. *Gaussian 03*, revision B.04; Gaussian, Inc.: Pittsburgh, PA, 2003.
(31) http://amber.scripps.edu/amber8.ffparms.tar.gz.
(32) Hoover, W. G. *Phys. Rev. A* **1985**, *31*, 1695.
(33) Melchionna, S.; Ciccotti, G.; Holian, B. L. *Mol. Phys.* **1993**, *78*, 533.
(34) Nosé, S. *J. Chem. Phys.* **1984**, *81*, 511.
(35) Forester, T. R.; Smith, W. *DL_POLY 2.14*; CCLRC, Daresbury Laboratory: Cheshire, U.K., 1995.
(36) Berendsen, H. J. C.; van der Spoel, D.; van Drunen, R. *Comput. Phys. Commun.* **1995**, *91*, 43.
(37) Lindahl, E.; Hess, B.; van der Spoel, D. *J. Mol. Mod.* **2001**, *7*, 306.
(38) van der Spoel, D.; Lindahl, E.; Hess, B.; van Buuren, A. R.; Apol, E.; Meulenhoff, P. J.; Tieleman, D. P.; Sijbers, A. L. T. M.; Feenstra, K. A.; van Drunen, R. Berendsen, H. J. C. *Gromacs User Manual*, version 3.2; 2004.
(39) Essmann, U.; Perera, L.; Berkowitz, M. L.; Darden, T.; Lee, H.; Pedersen L. G. *J. Chem. Phys.* **1995**, *103*, 8577.
(40) Alavi, S.; Thompson, D. L. *J. Chem. Phys.* **2005**, *122*, 154704.
(41) Velardez, G. F.; Alavi, S.; Thompson, D. L. *J. Chem. Phys.* **2003**, *119*, 6698.
(42) Solca, J.; Dyson, A. J.; Steinebrunner, G.; Kirchner, B. *Chem. Phys.* **1997**, *224*, 253.
(43) Solca, J.; Dyson, A. J.; Steinebrunner, G.; Kirchner, B.; Hubber, H. *J. Chem. Phys.* **1998**, *108*, 4107.
(44) Della Valle, R. G.; Venuti, E. *Phys. Rev. B* **1996**, *54*, 3809.
(45) *CRC Handbook of chemistry and physics*; Lide, D. R., Ed.; CRC Press: Boca Raton, FL, 1998.
(46) Luo, S. N.; Ahrens, T. J.; Çagin, T.; Strachan, A.; Goddard, W. A., III; Swift, D. C. *Phys. Rev. B* **2003**, *68*, 134206.
(47) Kintzinger, J. P.; Lehn, J. M.; Williams R. L. *Mol. Phys.* **1969**, *17*, 135.
(48) Agrawal, P. M.; Rice, B. M.; Thompson, D. L. *J. Chem. Phys.* **2003**, *118*, 9680.